Vibrational spectral diffusion and population dynamics in a glass-forming liquid: Variable bandwidth picosecond infrared spectroscopy

A. Tokmakoff, R. S. Urdahl, D. Zimdars, R. S. Francis, A. S. Kwok, and M. D. Fayer
Department of Chemistry, Stanford University, Stanford, California 94305

The temperature-dependent vibrational population dynamics and spectral diffusion of the CO stretching mode of tungsten hexacarbonyl in 2-methylpentane are observed from the room temperature liquid to the low temperature glass using picosecond infrared transient grating and pump–probe experiments. These experiments were performed between 10 and 300 K on the triply degenerate T_{1u} asymmetric CO stretching mode at 1984 cm^{-1} using pulses with bandwidths narrower and wider than the absorption bandwidth of the transition. The rate of vibrational population relaxation ($100 \leqslant T_1 < 150$ ps) is observed to *decrease* with increasing temperature. The orientational dynamics for this transition are observed on a faster time scale than the population relaxation. Although the liquid viscosity changes over 14 orders of magnitude, the orientational relaxation rate slows by less than one order of magnitude over the full temperature range. By comparing polarization-dependent experiments performed with both narrow and broad bandwidth transform-limited pulses, it is possible to measure temperature-dependent spectral diffusion in both the liquid and the glass. The spectral diffusion and the orientational relaxation are shown to be intimately related. It is proposed that both arise from the time evolution of the superposition of the three degenerate states created by the excitation pulse. © *1995 American Institute of Physics.*

I. INTRODUCTION

The absorption line shape of a vibrational transition in amorphous condensed matter systems has contributions from a variety of dynamic processes, including vibrational pure dephasing, vibrational population relaxation, and orientational relaxation. Each of these processes involve coupling between the internal vibration of a molecule and the external degrees of freedom of its environment. However, since vibrational lines of polyatomic molecules in polyatomic solvents are often inhomogeneously broadened,[1–5] analysis of line shapes measured by linear spectroscopy cannot provide information on dynamics.[6] A static (or slowly evolving) distribution of transition energies hides the dynamics that determine the homogeneous line shape. Nonlinear vibrational spectroscopies are required to determine the homogeneous vibrational line shape.[6,7] Even in the absence of inhomogeneous broadening, the measurement of the homogenous absorption line cannot distinguish the contributions of pure dephasing, population lifetime, and orientational relaxation. For vibrational transitions, all of these dynamics can contribute significantly to the observed homogeneous linewidth.

Time resolved infrared (IR) experiments performed on the ps and fs time scales can independently examine pure dephasing, population relaxation, and orientational relaxation. IR photon echo experiments can determine the homogeneous line shape of an inhomogeneously broadened transition.[2,3] IR pump–probe or transient grating experiments can measure population relaxation, and when performed with polarization selectivity, they can also measure orientational relaxation. In this paper, we demonstrate for the first time that it is also possible to measure spectral diffusion by employing polarization-selective transient grating or pump–probe experiments with transform-limited pulses of variable spectral bandwidth.

Vibrational spectral diffusion is the name given to evolution of the vibrational energy level splittings on a time scale long compared to that of the homogeneous dephasing time. The homogeneous dephasing, which arises from fast solvent fluctuations, is the inverse of the homogeneous line shape and is the observable of the photon echo experiment. In a liquid, the homogeneous vibrational linewidth can be much narrower than the inhomogeneous linewidth, even at room temperature.[3–5] However, on some time scale, a molecule in a liquid will sample all possible solvent environments that give rise to the distribution of transition energies underneath the inhomogeneous spectrum. Therefore, on a time scale long compared to the homogeneous dephasing time, the homogeneous vibrational line for a given molecule will spectrally diffuse throughout the full inhomogeneous line. The slow dynamic processes that give rise to spectral diffusion can appear static on the time scale of the homogeneous dephasing, and appear as part of the quasistatic inhomogeneous background. This quasistatic distribution of vibrational energies is rephased in a photon echo experiment and does not contribute to the homogenous linewidth. In a glass, which is a nonequilibrium time-evolving amorphous solid, spectral diffusion can also occur.[8] However, the entire inhomogeneous line may not be sampled except on an essentially infinite time scale.

The study of vibrational population relaxation dynamics in condensed phases gives insight into the coupling of discrete vibrational modes with the heat bath.[9,10] Population in excited vibrational modes must relax by transferring energy to other modes of the bath. This energy redistribution among vibrational modes has been observed for a number of systems.[11–18] Energy relaxation is accomplished via the coupling of modes through anharmonic pathways.[19–24] These couplings are sensitive to the environment of the vibrational mode of interest, which consists of the discrete vibrational

modes and structure of the solute and solvent, orientational dynamics of the molecules, and the continuum of collective solvent modes. These collective modes are referred to as phonons in solids and can be described as instantaneous normal modes (INM) in liquids. The efficiency of coupling, and therefore the rate of vibrational population relaxation, is dependent on the thermal population of the participating modes.[10,24]

To gain understanding of the wide range of variables describing vibrational population dynamics, temperature-dependent experiments are particularly important. Such experiments are sensitive both to the thermal occupation of modes involved in relaxation pathways, as well as the changing physical state of the system, such as phase transitions, density, and viscosity. Despite the great importance for understanding the role of physical structure and dynamics on vibrational coupling and on processes such as chemical reactivity[25] and electron transfer,[26] few studies have looked at temperature-dependent vibrational dynamics in condensed phases. Studies of this nature have been performed with ps and fs coherent Raman scattering[27] and infrared hole-burning.[28–31] Third-order coherent Raman experiments measure the Fourier transform of the entire vibrational spectral line, and therefore cannot discriminate between inhomogeneous and homogeneous broadening.[6] While persistent holeburning is a line narrowing technique, it cannot separate contributions from lifetime, homogeneous dephasing, and spectral diffusion. These problems can be overcome with time-resolved resonant infrared experiments. Picosecond infrared studies of temperature-dependent vibrational dynamics reported until now have observed the vibrational population lifetimes of discrete vibrations,[2,24,32,33] and used infrared photon echoes to observe the vibrational homogeneous linewidth in liquids and glasses.[2–4] In addition, picosecond transient holeburning has been used to observe transient holes and inhomogeneous broadening in a polymer as a function of temperature.[34]

In this paper, the results of measurements of temperature-dependent spectral diffusion, population relaxation, and orientational relaxation of a vibrational transition in a glass-forming organic liquid are presented. The T_{1u} CO stretching vibration (1980 cm^{-1}) of tungsten hexacarbonyl [$W(CO)_6$] in 2-methylpentane (2-MP) is observed from 300 K to 10 K using picosecond infrared transient grating and pump-probe experiments. This work is complementary to our recent description of the temperature dependence of the homogeneous vibrational linewidth in this system.[3,5] The temperature range studied here spans the transition from liquid to glass, and the transition from a homogeneously broadened vibrational transition to a massively inhomogeneously broadened line. The vibrational relaxation dynamics of metal carbonyl solutions at room temperature have been investigated at great length by Heilweil and co-workers.[15,18,35–37]

The population relaxation time for this system exhibits a counterintuitive temperature dependence, with relaxation times T_1 increasing with temperature. This behavior has also been recently reported for the system $W(CO)_6$ in $CHCl_3$ (Ref. 24) and is explained in terms of the temperature-dependence of three factors, thermal populations of low fre-

quency phonons (or INMs) of the liquid, the phonon density of states, and the anharmonic coupling matrix elements for the relaxation process.

The experiments presented are sensitive to the measurement bandwidth. Two distinct, transform-limited bandwidths were used. The broad bandwidth (short) pulse is wider than the vibrational spectral line, and thus observes the population dynamics of the entire line. Therefore, population relaxation and orientational relaxation will influence the time dependent observables, but spectral diffusion will not. The narrow bandwidth (long) pulse is significantly narrower than the vibrational linewidth. Therefore, excitation of the inhomogeneous line burns a transient polarized hole in the spectrum. This hole can fill in by population relaxation, orientational relaxation, and spectral diffusion, which redistributes the initial hole area across the entire line. The results observed up to 200 K with narrow bandwidth excitation are characteristic of spectral diffusion in the glass and liquid and are consistent with the inhomogeneous broadening of the transition.[3] The time scale and temperature dependence of the spectral diffusion are found to be equal to those of the orientational relaxation. This suggests that the orientational relaxation and spectral diffusion are intimately related. The orientational relaxation and spectral diffusion observed at temperatures below 200 K are independent of the macroscopic structural evolution of the solvent as shown by the fact that the solvent viscosity increases by more than 14 orders of magnitude while the orientational relaxation time increases by less than one order of magnitude. The similarity of the orientational relaxation dynamics and the spectral diffusion suggests a common mechanism that involves the time evolution of the superposition of the three T_{1u} modes that is prepared by the excitation pulse.

These experiments constitute time-resolved evidence for vibrational spectral diffusion. The change of the homogeneous linewidth with temperature for this system measured by photon echo experiments has been reported recently.[3] The results presented here and a new detailed analysis of the photon echo results[5] confirm the observation of a transition from a massively inhomogeneously broadened line in the low-temperature glass, to a significantly inhomogeneously broadened line in the low temperature liquid, and finally to a homogeneously broadened line at room temperature.

In addition, the results presented here are the first use of picosecond infrared transient gratings in condensed phase vibrational spectroscopy. The data show the great sensitivity enhancement of this technique over conventional pump–probe experiments for detecting small population transients. Previous midinfrared four-wave-mixing experiments on condensed-phase molecular vibrations have included photon echoes[2,3,5] and sum-frequency detected photon echoes on Si–H surface vibrations.[38]

II. EXPERIMENTAL PROCEDURES

The infrared transient grating and pump–probe experiments used to determine spectral diffusion, population relaxation, and orientational dynamics were performed with two sources of picosecond infrared pulses. Narrow bandwidth measurements were made using 10 ps pulses generated with

an optical parametric amplifier (OPA), while broader band-width measurements were made with 1.3 ps pulses from the Stanford superconducting-linear-accelerator-pumped free electron laser (FEL). The pulses from each source were observed to be nearly transform limited.

A LiIO$_3$ OPA was used to generate 10 ps, 1.5 cm^{-1} FWHM, tunable midinfrared pulses at 900 Hz. This system was modified from one described previously.[24,39] Briefly, the pulse train of a Q-switched, mode-locked, cavity-dumped Nd:YAG laser with a 10% output coupler is doubled and synchronously pumps a Rhodamine B dye laser with a Malachite Green saturable absorber cell. The dye laser and the Nd:YAG laser are cavity-dumped simultaneously to form the idler and pump pulses for the OPA. The cavity-dumped pulse of the Nd:YAG is frequency-doubled (532 nm, 65 ps, 400 μJ), and the remaining fundamental is frequency-doubled again to amplify the dye pulse in a single-stage double-pass amplifier yielding tunable dye pulses of 10 ps, 6 μJ at $\lambda \approx 595$ nm. The 532 nm pulse and the amplified dye pulse are made time coincident and are mixed in a 30 mm LiIO$_3$ crystal generating ~ 1 μJ, 10 ps pulses at $\lambda \approx 5.05$ μm with a 900 Hz repetition rate. The mid-IR is tuned by tuning the dye laser frequency with a 100 μm étalon. The mid-IR pulse is separated from the visible pulses with a CaF$_2$ Brewster prism. A 2% coated ZnSe beamsplitter is used to split off an intensity reference signal, which is monitored with a liquid-nitrogen-cooled HgCdTe detector.

The Stanford FEL was used as the source of 1.3 ps pulses at the same frequencies as the OPA. A detailed description of the optical setup will be given elsewhere.[5] The FEL emits a 2 ms macropulse at a 10 Hz repetition rate. Each macropulse consists of ~ 0.5 μJ micropulses at a repetition rate of 11.8 MHz. The micropulses were observed to be transform limited Gaussian pulses by performing autocorrelations in AgGaSe$_2$ and taking spectra with a 1 m grating monochromator. The bandwidth was measured as ~ 12 cm^{-1}. The macropulse was intensity stabilized by a germanium acousto-optic modulator (AOM) feedback system. The micropulse repetition rate of 11.8 MHz within the macropulse was reduced to 50 kHz by single-pulse selecting one pulse out of every 120 with a germanium AOM, making the effective experimental repetition rate 1 kHz. All data was taken with the 50 kHz or lower repetition rate to avoid thermal artifacts. The FEL intensity is monitored with a liquid-nitrogen-cooled HgCdTe detector after a 2% ZnSe beamsplitter. The pulse length (bandwidth) of the FEL is tunable from ~ 0.7–1.5 ps (20–10 cm^{-1}).

In the transient grating experiment,[40] the mid-IR beam is split into three equal portions. Two time coincident excitation (pump) pulses are crossed in the sample at an angle θ. The two beams produce a sinusoidal interference pattern in the sample with a fringe spacing of $d = \lambda / 2 \sin(\theta/2)$. Absorption of the infrared light by the T_{1u} CO stretching mode images the optical interference pattern into the sample. This produces a population diffraction grating. A third, time-delayed probe pulse is diffracted off the grating at the Bragg angle. The diffracted probe beam monitors the decay of the grating caused by population relaxation or other dynamic phenomena. The diffracted probe is detected in a unique direction

against zero background. The intensity of the diffracted probe signal is proportional to the square of the polarization induced by the probe pulse. For an experiment in which there is only population relaxation, the signal is proportional to the square of the excited state population and decays with twice the population decay rate constant.

The transient grating beams are focused to 200 μm with a 114 mm off-axis parabolic reflector. A second parabolic reflector after the sample serves to collimate the beams and the grating signal, and a third parabolic reflector then focuses all beams into another HgCdTe signal detector. The grating signal is easily found by rising off the three input beams, leaving the signal free to reach the detector. The grating signal detector is sampled by a gated-integrator and normalized to the cube of the mid-IR intensity with an analog signal processor. Further sensitivity is obtained by chopping one of the grating excitation beams and detecting through a lock-in amplifier.

For the pump–probe experiment, 10% of the IR beam is split off as the probe beam and sent through an optical delay line. The remainder is used as the pump beam. Both beams are focused to 200 μm in the sample with the same parabolic reflector as the transient grating. The intensity changes in the probe pulse with probe delay are detected with the HgCdTe signal detector. Pump–probe (transient absorption) data are collected by measuring a shot-normalized absorption change in the probe pulse with and without the pump beam, as described previously.[24]

For both experiments, polarization selectivity was used to distinguish contributions from orientational relaxation effects. In these experiments, pump and probe beams were polarized with ZnSe Brewster plate polarizers with extinction ratios of 3600:1. Experiments were performed with parallel pump and probe polarizations (0°), as well as magic angle probing where the probe beam polarization was rotated to 54.7° from the pump polarization. Probing at the magic angle has the effect of eliminating the influence of orientational relaxation on the signal in both the pump–probe[41] and transient grating[42,43] experiments.

Both W(CO)$_6$ and 2-MP were purchased as >99% pure and used without further purification. Data was taken on 6×10^{-4} M solutions of W(CO)$_6$ in 2-MP, corresponding to a mole fraction of <10^{-4}. At this concentration, the samples had a optical density of ~ 0.8 using a 400 μm path length. This concentration is sufficiently low that Förster excitation transfer does not occur between W(CO)$_6$ molecules.[35] The sample was placed between two CaF$_2$ flats spaced with a 400 μm Teflon gasket. Using indium wire, the windows were sealed vacuum tight to a copper block mounted on the cold finger of a closed cycled helium refrigerator. The temperature of the sample was measured to ± 0.2 K with a silicon diode sensor mounted on the CaF$_2$ flats with silver paste. The temperature gradient across the entire sample cell at all temperatures was <0.2 K after equilibration. Data were taken with decreasing temperature and the mid-IR frequency was tuned to follow the small temperature-dependent changes in the position of the absorption maxima.

Temperature-dependent IR absorption spectra of the W(CO)$_6$ in 2-MP solution were taken with a Mattson Re-
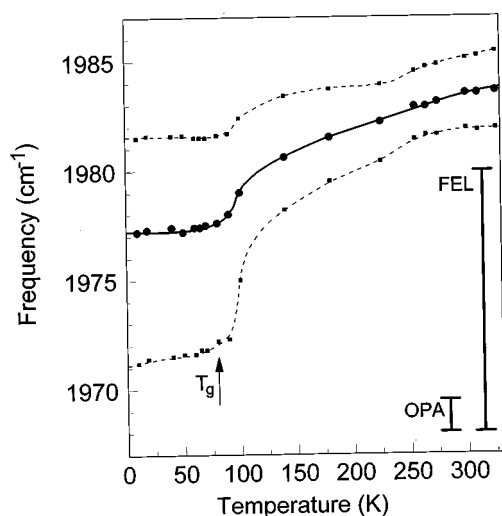
FIG. 1. Summary of the temperature-dependent IR absorption spectra of the T_{1u} CO stretching mode of $W(CO)_6$ in 2-MP. Circles represent the absorption maximum of the line. Small squares represent the half height frequencies on either side of the line. Lines have been drawn through the points as a guide for the eye. The line shape varied from a Voight profile in the high temperature liquid to a asymmetric Gaussian in the glass. For illustration purposes, the FWHM bandwidths of the two transform-limited ps IR sources are given by the vertical bars. The glass transition temperature of $T_g=79$ K is marked with an arrow.

search Series FTIR Spectrometer. Spectra were taken with 0.25 cm^{-1} resolution with the same closed cycled helium refrigerator and sample used in the time-resolved experiments.

III. RESULTS

The temperature-dependent IR absorption spectra of the T_{1u} CO stretching mode of $W(CO)_6$ in 2-MP are summarized in Fig. 1. The absorption maximum (filled circles) shifts to lower frequency as the temperature is lowered in the liquid. Below the glass transition temperature, $T_g=79$ K,[44] the absorption maximum is constant at ~ 1977 cm^{-1}. The half-width at half-maximum for the blue and red sides of the transition are shown in small squares. The bandwidth is observed to broaden from 3.7 cm^{-1} at 300 K to 10.5 cm^{-1} at 10 K. [The laser bandwidths and absorption linewidths given here and in the following discussion are measured as the full-width at half-maximum (FWHM).] In addition, as the temperature is lowered, the band becomes increasingly asymmetric. The narrow bandwidth OPA ($\Delta\nu=1.5$ cm^{-1}) pulses are narrower than the vibrational line at all temperatures. The FEL produced relatively wide bandwidth pulses ($\Delta\nu=12$ cm^{-1}) that are wider than the line at all temperatures. The bandwidths of the lasers are illustrated by the vertical bars in Fig. 1.

Lifetime measurements on this system were subject to a number of power-dependent effects that mask the true $v=0\rightarrow1$ population dynamics, if high pump powers are used.[24,36] The use of high power excitation pulses on this system has been shown to off-resonantly pump population to higher vibrational levels,[17,45] causing nonexponential behavior in the observed population decay.[24,36] Furthermore, the

homogeneous dephasing times for this system are approximately equal to or longer than the pulse length at all temperatures,[3] allowing for coherent pumping of higher transitions. For these reasons, detailed power studies were performed for both the pump–probe and transient grating experiments over the entire temperature range. At total beam energies above 800 nJ, pump–probe and transient grating decays made with the OPA were observed to be highly non-exponential, due to population of vibrational levels higher than $v=1$, as previously observed for metal carbonyls in CCl_4 and $CHCl_3$.[17,24] Decays showed power-dependent behavior down to 100 nJ, with deviations from exponentiality gradually vanishing with decreasing pump energy in the room temperature liquid. Using the OPA, distinct nonexponential behavior was observed at lower temperatures, but further power studies over the entire temperature range revealed that this behavior was not power dependent. Pump–probe data could be obtained for pump powers down to 50 nJ; no difference was observed for the data between 100 and 50 nJ. The transient grating technique was used in order to extend the sensitivity range. Transient grating data was taken down to energies of 3 nJ per beam. This data showed no changes below 50 nJ of total beam energy, and the data was insensitive to changes in the probe energy. The grating and pump–probe experiments gave identical results at sufficiently low power. Taking into account that the peak intensity in the grating experiment is proportional to the square of the total pump energy, the power dependent effects for the pump–probe become negligible at ~100 nJ, based on the pump–probe and transient grating data. Final pump–probe data sets were taken with a total beam energy of 100 nJ and transient grating data was taken with 3 nJ excitation pulses and 20 nJ of probe energy. These data sets yielded the same population dynamics. Data taken with the FEL did not display the same sensitivity to power, presumably because of the greater bandwidth, which reduces the energy per unit wavelength. FEL pump–probe data were taken between 100 and 50 nJ, and no power dependent behavior was observed at either high or low temperatures.

Pump–probe data taken on $W(CO)_6$ in 2-MP with the broad bandwidth FEL in the parallel polarization geometry (0°) are shown in Fig. 2(a) for several temperatures in the liquid and glass. The decays are notably biexponential at high temperatures. As the temperature decreases, the amplitude of the fast component becomes smaller and the decay time of the fast component becomes longer. When these data were taken with magic angle probing (54.7°), as shown in a semilog plot in Fig. 2(b), a single exponential decay is observed. This single exponential decay is identical to the long component in the parallel geometry at all temperatures. Because the fast component observed with parallel probing vanishes with magic angle probing, it can be attributed to orientational relaxation. The slow decay corresponds to the vibrational population relaxation time, T_1.

The data taken with the FEL from 10 to 300 K is summarized in Fig. 3. Data taken with parallel probing (0°) were fit to a biexponential decay
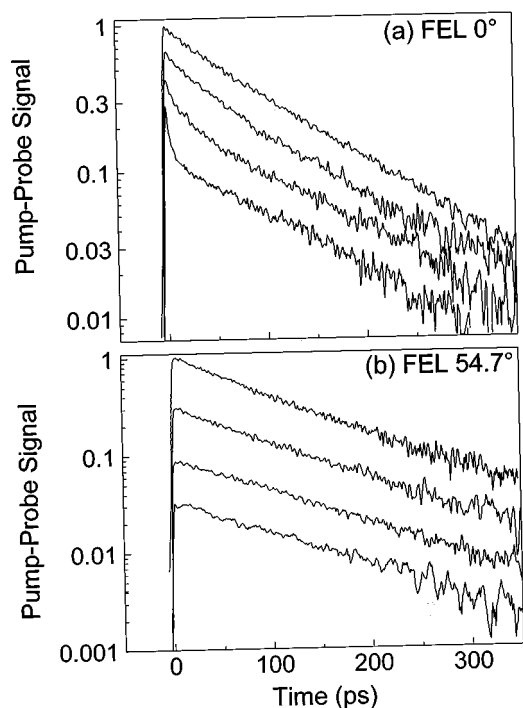
FIG. 2. (a) Semilog plot of temperature-dependent pump–probe data of the vibrational relaxation of the T_{1u} CO stretching mode of $W(CO)_6$ in 2-MP taken with the FEL using parallel pump and probe polarizations. The peak transient absorption signal is typically 5–10 mOD. Data sets were taken at temperatures of (from top) 40 K, 100 K, 200 K, 300 K. The decays are distinctly biexponential. (b) Semilog plot of pump–probe data taken with the FEL using magic angle probing. The data sets correspond to the same temperatures as in (a) and are (from top) 40 K, 100 K, 200 K, and 300 K. The decays are seen to be single exponential, and correspond to the long component of the biexponential observed in (a).

FIG. 3. Temperature-dependent vibrational relaxation data for pump–probe experiments performed with the FEL (t_p=1.3 ps, $\Delta\nu$=10 cm^{-1}), with representative error bars. (Top) Biexponential decay times for the pump–probe experiment. The long component (squares) is independent of polarization, while the short component (circles) disappears when magic angle (54.7°) probing is used. (Bottom) Relative zero-time decay amplitudes for the long and short components for parallel polarization (0°) probing data. The symbols correspond to the decay components above.

$$\frac{I(t)}{I_0} = (1-A)\exp(-t/\tau_{\text{slow}}) + A\,\exp(-t/\tau_{\text{fast}}), \qquad (1)$$

where $\tau_{\text{slow}} = T_1$, and τ_{fast} refers to the fast component of the pump–probe experiment due to orientational relaxation. The decay times T_1 and τ_{fast} are given in Fig. 3(a), and the corresponding decay amplitudes are shown in Fig. 3(b). The data taken at 54.7° was fit to a single exponential and reproduces the results of the long component in Fig. 3(a) exactly. The fast orientational component increases in rate with increasing temperature, and shows no discontinuity at the glass transition of 79 K. The amplitude of τ_{fast} is roughly constant with temperature in the liquid at approximately 44%. This is the fraction of the decay that is expected for full orientational randomization. Below ~125 K, the amplitude of the orientational component of the decay decreases. Orientational relaxation continues to exist in the glass, but τ_{fast} appears to be temperature independent.

The population relaxation time, T_1, *becomes faster* as the temperature is decreased in an approximately linear manner over the entire temperature range, with no discontinuity at the glass transition temperature. Since vibrational relaxation is expected to be a thermally activated process, this result is counterintuitive. Such a temperature dependence has also been observed recently for the system $W(CO)_6$ in $CHCl_3$.[24]
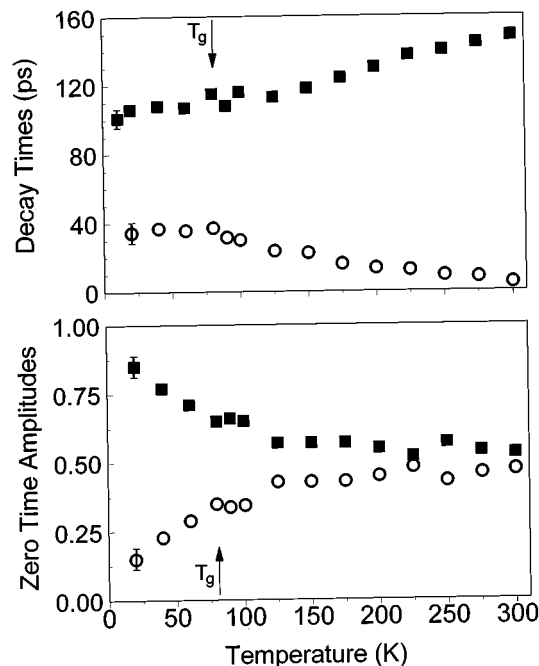
Pump–probe and transient grating data were taken on $W(CO)_6$ in 2-MP with the narrow bandwidth OPA pulses using both parallel and magic angle probing geometries. Parallel probe data displayed biexponential decays essentially identical to those seen with the FEL. With magic angle (54.7°) probing, between 300 K and ~200 K, single exponential decays were observed. However, below 200 K, *the decays became biexponential* with a fast decay component increasing in amplitude with decreasing temperature.

This behavior is shown in Fig. 4 for transient grating decays between 200 and 110 K. The data at 200 K is nearly exponential, but with decreasing temperature becomes increasingly nonexponential. The amplitude of the transient grating decay is proportional to the square of the excited state population.[40] Single exponential dynamics appears as a single exponential decay while biexponential dynamics appear as a biexponential squared. The transient grating data shown in Fig. 4 were taken with 3 nJ of pump energy per excitation beam. This can be compared with the 100 nJ of pump energy used for the pump–probe data in Fig. 2. These data demonstrate the enhanced sensitivity and signal to noise obtained with a transient grating experiment due to zero-background detection.

Transient grating and pump–probe data were taken at the magic angle with the OPA as a function of temperature between 10 and 300 K. The population dynamics observed with either experiment were the same, and are shown in Fig. 5. Data above 200 K were fit to a single exponential, while
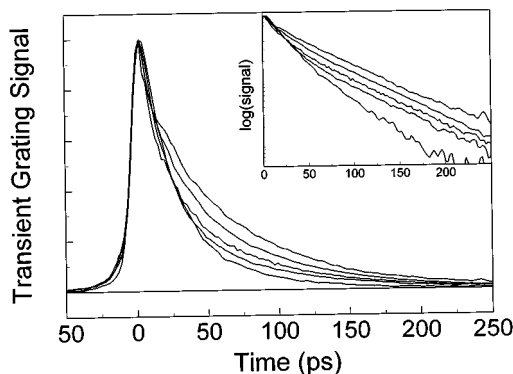
FIG. 4. Temperature-dependence of the transient grating signal taken with the OPA for temperatures between 200 and 110 K. The inset shows a semi-log plot of the data. The data sets correspond to temperatures of (from top) 200 K, 165 K, 150 K, 140 K, and 110 K. The decays are distinctly different from the pump–probe data, since the signal amplitude is proportional to the square of the excited state lifetime, whereas the pump–probe signal is linear. These data sets were taken with 3 nJ of energy per pump beam, demonstrating the transient grating's unique sensitivity due to zero-background detection.
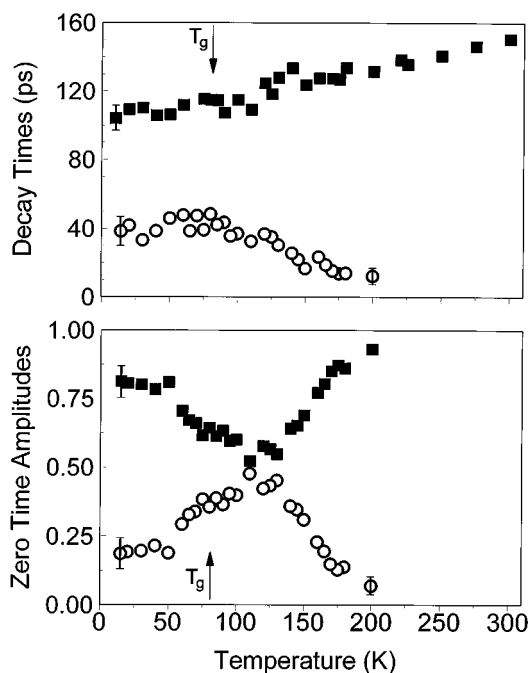

FIG. 5. Temperature-dependent vibrational relaxation data for magic angle transient grating and pump–probe experiments performed with the OPA (t_p=10 ps, $\Delta\nu$=1.5 cm^{-1}). All data points represent the average of several transient-grating and pump–probe data sets at that temperature. Representative error bars corresponding to the standard deviation of these measurements are shown. (Top) Biexponential decay times for the transient grating and pump–probe experiment. The long component (squares) becomes the single exponential in the high temperature liquid, and follows the population lifetime measured with the FEL experiment exactly. The short component (circles) appears at temperatures below ~200 K. The temperature dependence of the fast component closely follows that observed for the orientational relaxation observed with the FEL. (Bottom) Relative zero-time decay amplitudes for the long and short components for magic angle probing data above. The symbols correspond to the decay components above. The short component grows in amplitude as the temperature is dropped below ~200 K.

data below 200 K were fit to a biexponential. Pump–probe data were fit to Eq. (1); however, for direct comparison of decay constants, transient grating data were fit to

$$\frac{I(t)}{I_0} = [(1-A)\exp(-t/\tau_{slow}) + A \exp(-t/\tau_{fast})]^2. \quad (2)$$

The long component of the biexponential was averaged over several data sets at each temperature, using both the transient grating and pump–probe results. The averaged value of the long component was held fixed, and the amplitudes and decay time of the short component fit again. This reduced the number of parameters in the fits and improved the reliability of the fast decay constant and amplitude. The values of the slow and fast components of the biexponential are shown in Fig. 5(a). The amplitudes of these components are shown in Fig. 5(b). The decay times of the slow components of the biexponentials, τ_{slow}, reproduce the results of the population relaxation time (T_1) observed with the FEL for all temperatures. The decay times of the fast components follow the decay times of the orientational component observed with the FEL. However, it must be emphasized that the OPA (narrow bandwidth) data illustrated in Fig. 5 are taken with magic angle probing. When the data are taken with the FEL (broad bandwidth) at the magic angle, the decay is a single exponential at all temperatures. Therefore, the fast component cannot be orientational relaxation. The fast component in the OPA magic angle biexponential grows in amplitude as the temperature is dropped from 200 to 120 K. Below 120 K, the amplitude decreases with temperature. No discontinuities in either the decay times or amplitudes are observed near the glass transition temperature of T_g=79 K.

IV. DISCUSSION

A. Vibrational spectral diffusion

The careful power dependence study on the transient grating and pump–probe data demonstrates that the observed differences in the data taken with the FEL and OPA are representative of population dynamics of the vibrational transition. The only difference in the experiments are the pulse length and bandwidth of the excitation and probing sources. These parameters define the dimensions in time and frequency over which each experiment will be sensitive to population dynamics. The FEL produces short pulses with broader bandwidth, which allows enhanced temporal sensitivity, integrated over a wide frequency range. The OPA, with its longer pulses and narrower bandwidth, loses temporal resolution with the advantage of increased sensitivity to spectral dynamics. For spectroscopy on homogeneously broadened lines, enhanced spectral sensitivity at the expense of time resolution is no advantage. However, for inhomogeneously broadened lines, which are often the case for vibrational transitions in condensed phases,[2,3,5] narrow bandwidth
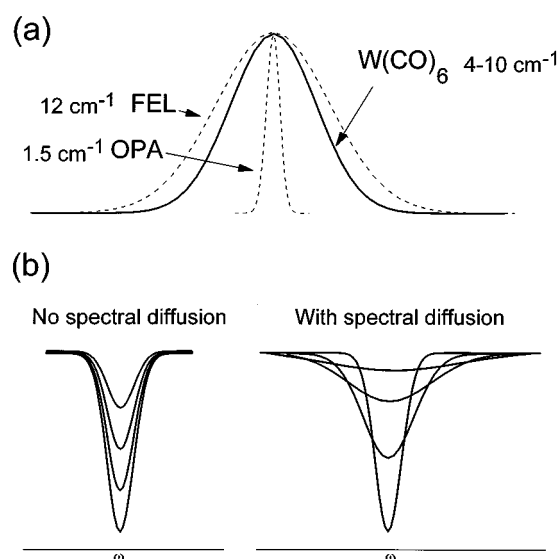
FIG. 6. (a) A schematic demonstrating the relative bandwidths of the FEL and OPA pulses, compared to the T_{1u} CO stretching vibration of $W(CO)_6$ in 2-MP. The case illustrated corresponds to the absorption linewidth in the 2-MP glass between 10 and 79 K. The OPA is narrower than the absorption linewidth at all temperatures, while the FEL is wider. (b) A diagram demonstrating the frequency domain behavior of the transient hole at various times in a narrow bandwidth transient grating or pump–probe experiment. With no spectral diffusion, the transient hole burned fills in exponentially. With spectral diffusion, the hole fills in the same manner due to population relaxation, but also spreads in frequency to assume the inhomogeneous linewidth at infinite time. These population dynamics, probed with the narrow bandwidth probe, would observe a biexponential decay.

experiments will be sensitive to spectral diffusion dynamics on time scales longer than the pulse duration.

Spectral diffusion refers to evolution of the transition energy on time scales longer than the homogeneous dephasing time, T_2. It is usually associated with slower solvent fluctuations and structural evolution. Spectral diffusion results in the sampling of a wider distribution of energies than the homogeneous width. For a homogeneously broadened line, all transition energies are sampled on the time scale of T_2. Thus, spectral diffusion only occurs in inhomogeneously broadened lines, i.e., the linewidth observed in an absorption spectrum is broader than the homogeneous linewidth measured in a photon echo experiment.

Spectral diffusion can occur over a great range of time scales, from the homogeneous dephasing time to days or even longer. This wide range of time scales is observed in low temperature crystals and glasses, in which local structural evolution occurs slowly.[8,46,47] In a liquid, local structures evolve rapidly and assume all possible configurations on short time scales, generally picoseconds at room temperature. Therefore, in liquids it is anticipated that spectral diffusion will occur relatively rapidly.

The differences in the population dynamics observed for the bandwidth-dependent FEL and OPA data at the magic angle are consistent with the observation of spectral diffusion in an inhomogeneously broadened line. Figure 6(a) shows a schematic representation of the bandwidths of the two infrared sources, compared to the IR absorption linewidth of the

T_{1u} CO stretching vibration of $W(CO)_6$ in 2-MP. The IR absorption bandwidth of the T_{1u} transition varies with temperature from a 3.7 cm^{-1} at 300 K to 10 cm^{-1} at 10 K. The spectral bandwidth of the FEL is $\Delta\nu=12$ cm^{-1}, so that pump–probe experiments performed with this source excite and probe population across the entire absorption line at all temperatures. However, the 10 ps OPA pulses have a bandwidth of $\Delta\nu=1.5$ cm^{-1}, which is narrower than the $W(CO)_6$ linewidth at all temperatures. Transient grating and pump–probe experiments with the OPA will bleach a transient hole in the absorption line corresponding to the homogeneous linewidth or the laser bandwidth, whichever is greater. If the homogeneous linewidth and the laser bandwidth are similar, the initial hole width is given by the convolution of the two. The dynamics of this hole are probed with the bandwidth of the probe pulse. When the line is inhomogeneously broadened, the transient hole in the absorption line will evolve due to population relaxation and spectral diffusion. This is shown schematically for the population hole bleached by the OPA in Fig. 6(b). For the case where spectral diffusion occurs at times long compared to the population relaxation, population relaxation will fill in hole with the excited state lifetime but not alter the shape of the hole in frequency. This hole filling will be observed as exponential signal decay. If spectral diffusion occurs on a time scale fast compared to the population relaxation time, the hole will spread in frequency, eventually assuming the shape of the entire inhomogeneous line. Since the probe spectrum is narrow compared to the inhomogeneous linewidth, the spectral diffusion will reduce the hole depth at the probe wavelength, causing the signal in a pump–probe or transient grating experiment to decay. The signal will not decay to zero since spreading of the hole over the entire inhomogeneous line still leaves some bleaching at the probe wavelength. The signal will then continue to decay to zero by the slower time scale population relaxation. If spectral diffusion and the lifetime are on the same time scale, then the hole will spread and decay simultaneously.

The magic angle data taken with the OPA shown in Fig. 5 represent the influence of spectral diffusion on the vibrational dynamics of a transition that becomes homogeneously broadened at room temperature. The OPA magic angle data are exponential and are identical to the magic angle data taken with the FEL, down to a temperature of 200 K. At this point, the OPA data becomes nonexponential, with a low amplitude, fast decay component appearing. This point represents the temperature at which the inhomogeneity in the vibrational line exists on the time scale of the 10 ps OPA pulses. At temperatures above 250 K, the line is homogeneously broadened. For a homogeneously broadened line, the pump pulse will bleach the entire line even though the OPA pulse bandwidth is less than the linewidth. The FEL pump pulse bleaches the entire line at all temperatures because its bandwidth is wider than the line. Thus spectral diffusion will have no influence on the FEL data, but can appear as an additional decay component in the magic angle OPA data.

The fact that the line is homogeneously broadened at and near room temperature, and only develops substantial inhomogeneity as the temperature is reduced below 200 K, is demonstrated by photon echo experiments on this sample.[3,5]
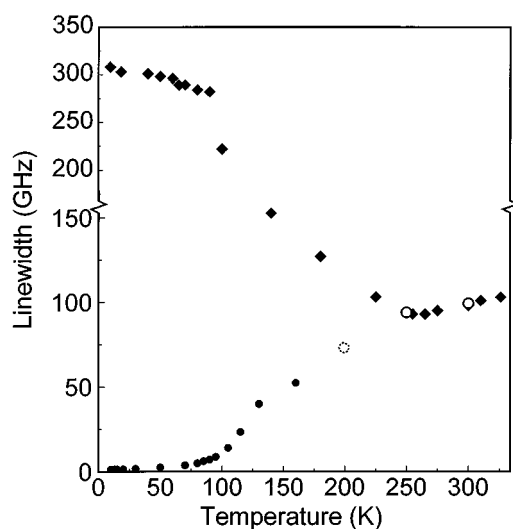
FIG. 7. Temperature dependence of the homogeneous and absorption linewidths for $W(CO)_6$ in 2-MP. The homogeneous linewidths (circles) were taken from photon echo data on this system (Ref. 3). The absorption linewidths (diamonds) are those taken from Fig. 1. The "echo" data at 250 and 300 K are really free induction decays that match the observed absorption line, showing the spectra are homogeneously broadened. At 200 K, the absorption line begins to display some inhomogeneous broadening. The error bars are approximately the size of the markers for the absorption data, and are approximately ±10% for echo data above 150 K.

Figure 7 displays photon echo measurements of the homogeneous linewidth (circles) taken on this sample with the FEL (Ref. 3) and the absorption spectrum linewidths (diamonds) from Fig. 1. (These data and photon echo data for other liquids and glasses will be discussed in detail elsewhere.[5]) While the echo signal can be resolved at all temperatures, the data at 300 K and 250 K actually represent the free induction decay (FID) of a homogeneously broadened line. This is shown by the fact that the FID decays yield linewidths that exactly match the absorption linewidths. The 200 K point represents the transition between homogeneous broadening at high temperatures and inhomogeneous broadening at lower temperatures. Thus the onset of the nonexponential magic angle OPA data coincides with the absorption line becoming inhomogeneously broadened.

Qualitatively, the amplitude of the spectral diffusion component of the OPA biexponential decay can be understood in the following manner. Above 200 K, the line is homogeneously broadened, and thus no spectral diffusion is observed. Although the bandwidth of the laser is less than the spectroscopic linewidth, the entire homogeneously broadened line is bleached uniformly. At 200 K, the line becomes inhomogeneous, although the homogeneous contribution still dominates. At this temperature, the hole bleached by the pump is almost as wide as the entire line. Rapid spectral diffusion filling of this hole does very little to reduce its depth across the probe pulse bandwidth. As the temperature is decreased from 200 K to ~120 K, the decrease in the homogeneous linewidth results in a deeper and narrower transient hole. A deeper initial hole, when spread over the increasing inhomogeneous linewidth, is observed as an increased amplitude in the spectral diffusion component. The

maximum amplitude of the spectral diffusion component of the decay occurs at ~120 K. At this temperature and below, the homogeneous line is narrower than the OPA pulse bandwidth, and the initial hole is constant at the laser bandwidth. As the temperature decreases further and the glass transition is approached, the viscosity increases dramatically and spectral diffusion no longer spreads the hole over the entire inhomogeneous line. This restricted spectral diffusion, discussed in detail below, decreases the amplitude of hole filling observed by the probe pulse. Thus, the amplitude of the spectral diffusion component of the biexponential decay decreases as the temperature is reduced below ~120 K.

The data presented here provide compelling evidence of spectral diffusion based on its temperature dependence, relationship to the orientational relaxation, independence of power dependent effects, and disappearance with the transition to a homogeneous vibrational line shape at high temperature. These experiments were conducted with two distinct bandwidths using the same bandwidth for pump and probe. Another way these experiments could be conducted is to use a narrow bandwidth pump and independently tunable narrow bandwidth probe or spectrally resolved broad bandwidth probe. This method allows the observation of the spectrum of the hole,[34,48,49] and could be used to observe the broadening of the hole with time.

B. Orientational relaxation

For pump–probe measurements taken with parallel polarization, the transient absorption, due both to orientational and population relaxation, is expected to decay as[41]

$$I(t) = I_0 \exp(-t/T_1)[1 + 2C(t)], \quad (3)$$

where $C(t)$ is the orientationally averaged Legendre polynomial of the dipole correlation function,

$$C(t) = \tfrac{2}{5} \langle P_2[\mu(0) \cdot \mu(t)] \rangle = \tfrac{2}{5} \exp(-6D_{or}t). \quad (4)$$

The final equality in this expression is the result obtained for the orientational diffusion of a spherical rotor in small steps, and the orientational correlation time is $\tau_{or} = 1/6D_{or}$. This is the case expected for the orientational relaxation of the initially excited $W(CO)_6$ dipole. From Eqs. (3) and (4), the pump–probe data are expected to decay as

$$\frac{I(t)}{I_0} = \frac{5}{9} \exp(-t/T_1) + \frac{4}{9} \exp\left[-t\left(\frac{1}{T_1} + \frac{1}{\tau_{or}}\right)\right]. \quad (5)$$

The decay is a biexponential, as observed with the FEL probing at 0°. When compared with Eq. (1), τ_{slow} gives the vibrational lifetime, T_1, and τ_{fast} is given by the sum of the rates for orientational and population relaxation. The orientational correlation times ($\tau_{or}^{-1} = \tau_{fast}^{-1} - T_1^{-1}$), calculated from the decay constants of the fast components of the 0° pump–probe data [see Fig. 3(a)], are shown in Fig. 8(a).

Equation (5) predicts that the zero-time amplitudes of the orientational relaxation component in the 0° FEL data should be equal to 4/9. As seen in Fig. 3(b), this amplitude is roughly constant at ~0.44 for temperatures in the liquid between 120 and 300 K. In this temperature range, the orien-
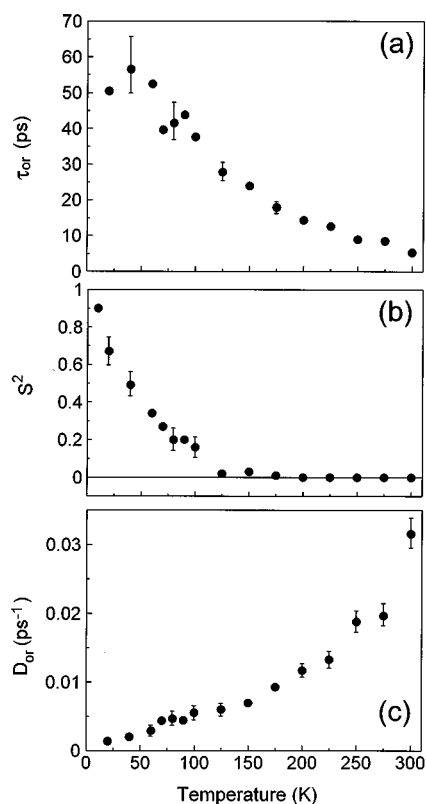
FIG. 8. Temperature-dependence of orientational relaxation parameters calculated from the fast decay components in Fig. 3(a). (a) Orientational diffusion time, τ_{or}. (b) Generalized order parameter, S^2. The point at 10 K is added as the minimum value of S^2 not discernible from the pump–probe data. (c) Orientational diffusion constant derived with the generalized order parameter in (b) using the expression given in Ref. 51. Complete orientational randomization was assumed for $T \leqslant 125$ K and orientational relaxation restricted to a cone was used for $T < 125$ K.

tational relaxation of the triply degenerate T_{1u} mode behaves in the expected manner. As shown in Fig. 3(b), below 120 K, the amplitude of the orientational component decreases. Note also that the amplitude of the fast spectral diffusion component of the OPA magic angle data, shown in Fig. 5(b), decreases in a similar manner. At high temperatures, the amplitude of the orientational component in the FEL data are consistent with complete orientational randomization of the dipole direction. The decrease in the orientational amplitude at low temperatures is caused by incomplete orientational relaxation.[50–54]

For restricted orientational relaxation, the dipole correlation function is assumed to be separable into independent "internal" and "external" motions, $C(t) = C_{\text{Ext}}(t) C_{\text{Int}}(t)$.[52,53] The internal partial reorientation is fast and limited by the long time evolution of the external solvent structure. This is the case in the very viscous liquid and glass ($T < 125$ K). In this picture, the dipole correlation function for the fast orientational relaxation within a cone is expected to decay exponentially to a nonzero value, S^2,[52]

$$C_{\text{Int}}(t) = S^2 + (1 - S^2)\exp(-t/\tau_{\text{or}}). \tag{6}$$

S is the generalized order parameter, which describes the degree of restriction on the orientational motion. S satisfies the inequality $0 \leqslant S^2 \leqslant 1$, where $S^2 = 0$ describes unrestricted

reorientation, while $S^2 = 1$ is no orientational motion. If the slow external contribution occurs on a time scale much longer than the vibrational lifetime, the pump–probe signal for restricted orientational motion is expected to decay as

$$\frac{I(t)}{I_0} = \left(\frac{5}{9} + \frac{4}{9} S^2\right)\exp(-t/T_1) + \left(\frac{4}{9} - \frac{5}{9} S^2\right)$$
$$\times \exp\left[-t\left(\frac{1}{T_1} + \frac{1}{\tau_{\text{or}}}\right)\right]. \tag{7}$$

Equation (7) shows that S can be obtained from the amplitudes of the pump–probe decay. The generalized order parameter calculated from the pump–probe amplitudes of the FEL 0° data are given in Fig. 8(b).

The restricted range of motion given by S, can be modeled as free diffusion of the excitation dipole within a cone of semiangle θ. This wobbling-in-a-cone model has been described in detail previously.[50,51,54] The cone angle can be determined from the generalized order parameter through the relation

$$S^2 = \left[\tfrac{1}{2}(\cos \theta)(1 + \cos \theta)\right]^2, \tag{8}$$

where $0 \leqslant \theta \leqslant 180°$. The orientational diffusion constant D_{or} is related both to θ and to τ_{or}. The general expression is lengthy and has been given by Lipari and Szabo.[51] For small cone angles ($\theta < 30°$), $D_{\text{or}} = 7\theta^2/24\tau_{\text{or}}$. For complete orientational randomization, $D_{\text{or}} = 1/6\tau_{\text{or}}$ is recovered.

The use of the wobbling in a cone model works well for obtaining orientational diffusion constants for motions restricted to cone angles smaller than $\sim 75°$.[52,55] As can be seen from Eq. (8), $S^2 < 0.02$ over the range $77° < \theta < 180°$, resulting in an uncertainty of $\sim 40\%$ in the $D_{\text{or}}\tau_{\text{or}}$ product over this range. At smaller cone angles, the value of θ is very sensitive to S^2. The amplitude of the orientational component of the decay gives S^2, and through Eq. (8), θ. The cone angle θ is related to the $D_{\text{or}}\tau_{\text{or}}$ product,[51] and with τ_{or}, D_{or} is obtained. The most accurate determination of D_{or} for restricted orientational relaxation is in the small cone angle limit.

The orientational diffusion constant is the true measure of the microscopic dynamics. To determine the temperature dependence of D_{or}, the pump–probe data at temperatures >120 K were treated as unrestricted orientational motion, while for temperatures <120 K, the data were treated as motion within a cone. The results are given in Fig. 8(c). Temperatures >120 K gave amplitudes expected for complete orientational randomization, and the diffusion constant was determined from $D_{\text{or}} = 1/6\tau_{\text{or}}$. For temperatures between 120 and 10 K, the amplitudes of the pump–probe indicate cone angles that vary from 75° to $<15°$. The diffusion constants were calculated from the relation given by Ref. 51.

C. Mechanism of orientational relaxation and spectral diffusion

It is important to emphasize again that the magic angle data taken with the broad bandwidth FEL pulses are always single exponential. Only the narrow bandwidth OPA magic angle data are biexponential. At all temperatures where the biexponential behavior is observed in the magic angle OPA
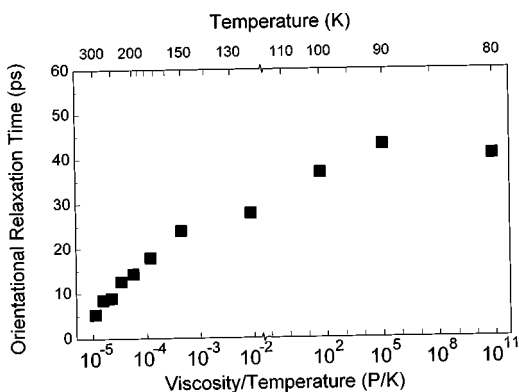
FIG. 9. Plot of the orientational relaxation time τ_{or} of $W(CO)_6$ in 2-MP as a function of the viscosity to temperature ratio (η/T) for data shown in Fig. 8(a). The data spans temperatures from 300 K to the glass transition temperature of 79 K. Hydrodynamic behavior predicts a linear relationship, yet the orientational relaxation time varies only by one order of magnitude for a η/T change of 16 orders of magnitude. Note that the η/T axis is logarithmic, with a change of scales at ~120 K, in order to display the data clearly.

data, the decay constants obtained for the fast spectral diffusion component match the orientational relaxation decay constants obtained from the 0° FEL data. This strongly suggests that the same mechanism is responsible for both the orientational relaxation and the spectral diffusion.

The orientational relaxation and associated spectral diffusion are uncorrelated with either the normal rotational diffusion of the $W(CO)_6$ or of the 2-MP solvent. This is demonstrated by the viscosity dependence of conventional rotational diffusion. The data taken in liquid 2-MP measure orientational relaxation of the excited transition dipole of the $W(CO)_6$ CO asymmetric stretch through a temperature range over which the solvent viscosity changes by greater than 14 orders of magnitude.[56] Debye–Stokes–Einstein (DSE) hydrodynamic theory gives the orientational correlation time for a spherical rotor as $\tau_{or} = V_{eff}\eta/kT$, where V_{eff} is the effective volume of the molecule and η is the viscosity. The DSE equation shows that rotational diffusion should slow by approximately 16 orders of magnitude over the temperature range of 300–79 K. Figure 9 displays a plot of τ_{or} as a function of η/T for the excited T_{1u} transition dipole in liquid 2-MP, as determined from the FEL pump–probe experiments. The orientational relaxation of the initially excited transition dipole slows by one order of magnitude over the temperature range in which η/T decreases by 16 orders of magnitude. This behavior is decidedly nonhydrodynamic and demonstrates that the orientational relaxation and associated spectral diffusion do not arise from conventional rotational diffusion.

The lack of correlation between the temperature dependence of the orientational relaxation rate and the viscosity shows that normal rotational diffusion is not occurring. A spherical molecule in a solvent can have slip boundary conditions and can be effectively decoupled from the solvent viscosity.[57] However, a space-filling model of $W(CO)_6$ shows that it is far from spherical. The carbonyls are large, nonoverlapping projections. The 2-MP solvent molecules are approximately the same size as the $W(CO)_6$. Therefore, nor-

mal stick boundary conditions should apply, and the boundary conditions are not an explanation for the nonhydrodynamic behavior.

To provide a consistent explanation for the complex dynamics observed in the variable bandwidth experiments, it is necessary to examine in some detail the nature of the T_{1u} state that is excited and probed in the experiments. Metal hexacarbonyls belong to the O_h point group, and the T_{1u} normal mode is an asymmetric CO stretching motion of opposite in-line carbonyl pairs.[58] The asymmetric stretches of the three pairs of carbonyl ligands are degenerate. If we take a molecular based orthogonal coordinate system, x, y, and z, with each of these three axes directed along one of the in-line pairs of carbonyls, then we can label three eigenkets of the triply degenerate manifold as $|X\rangle$, $|Y\rangle$, and $|Z\rangle$. These kets are taken to be normalized. Since these eigenkets are degenerate, any superposition of them is also an eigenket with the same eigenvalue. A superposition of these kets can be made to point in any direction in the molecular frame. For any such superposition state, two other orthogonal superpositions can then be formed to produce a set of normalized orthogonal triply-degenerate eigenkets.

The excitation pulse is polarized. In general, the orientation of the molecule will not place one of the molecular frame coordinates, x, y, or z, along the pump pulse E-field direction. The E-field will excite a superposition of the degenerate basis kets, $|X\rangle$, $|Y\rangle$, and $|Z\rangle$, to yield an initially excited state, $|S\rangle$, with an oscillating dipole along the E-field polarization,

$$|S\rangle = a|X\rangle + b|Y\rangle + c|Z\rangle. \tag{9}$$

Here, $|S\rangle$ is normalized, and in writing $|S\rangle$, the basis states were taken to be degenerate. On a short time scale, local directional anisotropy will exist in the intermolecular interactions of the $W(CO)_6$ and the solvent. This will break the degeneracy of the basis states.[59] However, as long as the splitting is small compared to the laser bandwidth or the Rabi frequency, a superposition described by Eq. (9) will be formed.

We propose a mechanism for orientational relaxation that does not involve the physical motion of the molecule, therefore decoupling orientational relaxation from the solvent. The decay of the transition dipole correlation function [Eq. (4)] gives rise to the orientational relaxation observable. The transition dipole is initially along the pump pulse E-field polarization and is associated with the superposition state $|S\rangle$ given in Eq. (9). Fluctuations in the solvent can cause the coefficients of the basis states that form $|S\rangle$ to evolve in time, i.e.,

$$|S\rangle = a(t)|X\rangle + b(t)|Y\rangle + c(t)|Z\rangle. \tag{10}$$

As the coefficients of the basis vector evolve in time, the direction of the transition dipole will also change direction. The transition dipole projection operator can be written as

$$\bar{\mu}|G\rangle\langle G|\bar{\mu}, \tag{11}$$

where $|G\rangle$ is the vibrational ground state, and $\bar{\mu} = \mu_x + \mu_y + \mu_z$. Then the projection of the transition dipole in terms of the basis states $|X\rangle$, $|Y\rangle$, and $|Z\rangle$ which are along the molecular axis, x, y, and z is

$$\langle S|\bar{\mu}|G\rangle\langle G|\bar{\mu}|S\rangle = \langle S|\mu_x|G\rangle\langle G|\mu_x|S\rangle + \langle S|\mu_y|G\rangle$$
$$\times \langle G|\mu_y|S\rangle + \langle S|\mu_z|G\rangle\langle G|\mu_z|S\rangle. \tag{12}$$

Since μ_x only couples $\langle G|$ to $|X\rangle$, the projection of the transition dipole on the x molecular axis is

$$P_x = \langle X|\mu_x|G\rangle a^*(t)a(t)\langle G|\mu_x|X\rangle \propto |a(t)|^2. \tag{13a}$$

Similarly, we write

$$P_y = \langle Y|\mu_y|G\rangle b^*(t)b(t)\langle G|\mu_y|Y\rangle \propto |b(t)|^2, \tag{13b}$$

$$P_z = \langle Z|\mu_z|G\rangle c^*(t)c(t)\langle G|\mu_z|Z\rangle \propto |c(t)|^2. \tag{13c}$$

The proportionality constant is the same for each projection and $|a(t)|^2 + |b(t)|^2 + |c(t)|^2 = 1$. Thus it can be seen that the direction of the transition dipole will evolve in time because of the changing composition of the excited superposition state even though the molecule itself undergoes *no physical rotation*. This explains the nonhydrodynamic origin of the orientational relaxation. Although the viscosity changes 14 decades in going from room temperature to the glass transition temperature, the decrease in the rate of orientational relaxation is very mild as can be seen from the plot of the orientational relaxation diffusion constant shown in Fig. 8(c). The relaxation caused by the evolution of the superposition state is much faster than the rotational diffusion at all temperatures except perhaps room temperature.

Above ~ 150 K, complete orientational randomization occurs. This is demonstrated by the magnitude of the fast component of the biexponential 0° FEL data in Fig. 3. The time-dependent coefficients in Eq. (10) completely randomized because of interactions of the vibration with the fluctuating solvent structure. At lower temperatures, the orientational randomization is incomplete. This was described above in terms of the wobbling-in-a-cone model. Previously, the cone model has been applied to the actual physical motion of a molecule restricted within a certain range of angles, whereas here it is the evolution of the coefficients in the superposition state that is restricted. Incomplete orientational relaxation implies that the coefficients do not completely randomize.

In the supercooled liquid and in the glassy state, structural evolution of the solvent is greatly hindered and can occur over a vast range of times scales. Fast structural changes for two level systems with small barriers can occur on a ps time scale, while slower structural evolution can occurs on the time scale of seconds,[8] hours,[60] weeks,[61] and perhaps geological time scales. Therefore, it is possible for there to be a restricted set of local structural changes that result in only partial randomization of the superposition state coefficients on the time scale of the measurement. On a longer time scale, large barriers may be surmounted, and further structural evolution can result. However, if this longer time scale is long compared to the excited state lifetime, only partial orientational randomization will occur, re-

sulting in the cone of orientations. This behavior occurs in both the supercooled liquid and the glass. As the temperature is lowered, the range of structures that are sampled on a fast time scale decreases, and the cone angle becomes smaller. The restriction on the orientational relaxation only becomes significant when the glass transition is approached, and it becomes very pronounced in the glass. At the lowest temperature, 10 K, within experimental error, no orientational relaxation occurs.

As shown above, the spectral diffusion seen in the fast component of the OPA magic angle biexponential decay is identical to the orientational relaxation in time dependence and temperature dependence. This is true even to the point that the extent of spectral diffusion begins to decrease as the glass transition temperature is approached, decreases substantially as the temperature of the glass is lowered, and ceases at 10 K within experimental error. Therefore, it is reasonable to propose that the structural fluctuations responsible for spectral diffusion are the same as those responsible for the superposition-state-evolution-induced orientational relaxation. Spectral diffusion is caused by the evolution of the energy eigenvalue of the state, $|S\rangle$. The anisotropic interactions of $|S\rangle$ with the medium will determine its energy as well as break the degeneracy. Spectral diffusion can be caused by both the time-dependent fluctuations in the energy center of gravity of $|S\rangle$ and by fluctuations in the splittings of the three states. At sufficiently high temperatures, 200 K to ~ 120 K, the fluctuations in the energy are sufficient to sample the entire inhomogeneous line, and complete spectral diffusion occurs. At lower temperatures, restricted solvent structural evolution results in partial spectral diffusion, in a manner analogous to the incomplete orientational relaxation.

Another way to consider the spectral diffusion is as a direct result of the orientational relaxation. As the coefficients in the superposition state evolve in time, the direction of the transition dipole changes. This means that the direction of the actual vibrational motion is changing. In an anisotropic environment, a change in the direction of vibration will result in a change in the vibrational potential. As the vibrational potential evolves, so does its energy. Thus, the orientational relaxation and the spectral diffusion are manifestations of the same microscopic dynamics, and their time and temperature dependencies are identical.

D. Temperature dependence of the vibrational lifetime

The temperature dependence of the population lifetime (T_1) of the T_{1u} CO stretching mode observed by the FEL and OPA in Figs. 3(a) and 5(a) is counterintuitive. The lifetime actually becomes longer as the temperature is raised. This behavior was also recently observed for solutions of $W(CO)_6$ in $CHCl_3$.[24] Vibrational relaxation is expected to be a thermally activated process; as the low frequency modes that couple to the initially excited vibration become thermally populated, the rate of relaxation is expected to increase. In the $W(CO)_6$/2-MP system, energy from the initially excited CO stretch will relax into other discrete modes of $W(CO)_6$ and solvent vibrational modes Energy mismatch is made up by the excitation of low frequency modes of the solvent continuum (instantaneous normal modes or "phonons"). The

initial excitation can relax into modes such as the other carbonyl stretches, W–C stretches and WCO bends, as well as the intermolecular solvent vibrational modes and phonons.

More precisely, the temperature-dependence of vibrational relaxation is an anharmonic process in which the temperature-dependence of the phonon density of states, phonon thermal occupation numbers, and anharmonic coupling matrix elements must be considered. As an example, consider the lowest order cubic process. For a cubic relaxation process, in which a vibrational quantum relaxes from the initially excited state of frequency Ω to a lower frequency vibration, ω, through emission of a phonon, $\omega_{ph} = \Omega - \omega$, the rate of the relaxation process is given by[10,24]

$$K = \frac{2\pi}{\hbar} \rho_{ph} |\langle V^{(3)} \rangle|^2 (1 + n_{ph})(1 + n_\omega). \tag{14}$$

Here ρ_{ph} refers to the phonon density of states at ω_{ph}, $\langle V^{(3)} \rangle$ is the cubic anharmonic coupling matrix element, and n is the thermally averaged occupation number

$$n_i = [\exp(\hbar \omega_i / kT) - 1]^{-1}. \tag{15}$$

For a high frequency vibration, such as the T_{1u} CO stretching mode, both Ω and ω are much greater than $kT/\hbar$. Thus, n_ω in the last term in Eq. (14) is negligible. Since vibrational relaxation occurs through multiple channels, the observed rate is a sum over all vibrational and phonon frequencies for all cubic and higher order processes that satisfy the energy conservation requirement, $\Omega = \Sigma \omega + \Sigma \omega_{ph}$.

Equation (14) demonstrates that the temperature dependence of the cubic anharmonic relaxation mechanism will be determined by the temperature-dependence of the phonon occupation number, the phonon density of states, and the cubic anharmonic coupling matrix element.[24] The phonon thermal occupation will cause the relaxation rate to increase as a function of temperature. Thus to obtain an inverse temperature dependence, the remaining terms must overcome the thermal increase in rate. Both the phonon density of states and the cubic anharmonic coupling matrix element are sensitive to the nature of the liquid potential, and are thus density-dependent terms. The temperature dependence of these terms is expected to manifest itself through the density changes with temperature in the liquid and glass.

Although the temperature dependence of the phonon density of states in crystals is expected to increase in crystals,[62] the nature of low frequency modes in liquids are substantially different. The structure of liquids is not fixed, but evolves over many time scales. The low frequency modes of a liquid do not arise from delocalized lattice modes, as in crystals, but rather have contributions from librational, orientational, and translational motion of the solvent. Recent molecular dynamics calculations of the temperature-dependent density of states for instantaneous normal modes of liquid CS_2 (Ref. 63) and CCl_4 (Ref. 64) predict that the density of states increases with increasing temperature at lower frequencies (<40 cm^{-1}) while decreasing with temperature at higher frequencies. Thus the frequency of the phonons involved will determine what temperature dependence of ρ_{ph} is. Based on these findings, it is reasonable to assume that a decrease in the liquid density

of states in 2-MP can contribute to the inverse temperature dependence of the vibrational relaxation rate.

The cubic anharmonic coupling matrix element, $\langle V^{(3)} \rangle$, is not expected to be temperature-dependent; however, it is also expected to be sensitive to density changes in the liquid and glass. Calculations for molecular crystals have shown that anharmonic coupling matrix elements increase with density,[65] so that the thermal decrease in density may be able to overcome the thermal increase in vibrational relaxation rate. Thus, thermal occupation numbers increase with increasing temperature, but the density of states and the anharmonic coupling matrix elements can decrease with temperature. The competition between these factors will determine the temperature dependence of the vibrational relaxation. Identical considerations hold for higher order processes (quartic, etc.). If a decrease in density of states and coupling matrix elements is sufficiently large to overcome the increase in n_{ph} with increasing temperature, the vibrational lifetime will increase, as observed in Figs. 3(a) and 5(a).

V. CONCLUDING REMARKS

The temperature-dependent vibrational population dynamics of the triply degenerate T_{1u} CO stretching mode of $W(CO)_6$ in 2-MP, observed with variable bandwidth picosecond IR experiments, yield a number of fundamental insights into the nature of vibrational dynamics in condensed phases. Variable bandwidth experiments are sensitive to the different time and frequency dynamics contained within an inhomogeneously broadened vibrational line. Although time resolution is sacrificed with longer pulses, the narrower bandwidth is sensitive to spectral diffusion dynamics throughout the inhomogeneous line. For the $W(CO)_6$ in 2-MP, the use of variable bandwidth experiments provides insight into the relationship between spectral diffusion and the orientational motion of the T_{1u} vibration. The same time and temperature dependencies for these two observations demonstrate that they are manifestations of the same microscopic dynamics. Orientational motion of the CO stretch under the inhomogeneously broadened line is observed as spectral diffusion of the transient hole bleached by narrow bandwidth excitation. We have proposed that the mechanism for orientational motion and spectral diffusion in the liquid and glass is through the time evolution of the coefficients of the superposition state of the three orthogonal T_{1u} modes initially excited by the pump pulse.

The observation that the vibrational lifetime of $W(CO)_6$ in 2-MP actually becomes longer as the temperature increases demonstrates that temperature-dependent lifetimes cannot be described by an activation energy. Even in a system that shows a decrease in vibrational lifetime with increasing temperature, it is unrealistic to assign an activation energy based solely on the data. To understand condensed phase vibrational relaxation dynamics, it is necessary to consider the temperature dependencies of the thermal populations of low frequency modes of the liquid, the solvent density of states, and the anharmonic coupling matrix elements.

The experiments presented above suggest a number of different research directions that are currently being pursued. The orientational and spectral diffusion dynamics are domi-

nated by the triply degenerate nature of the T_{1u} mode. Temperature-dependent experiments with a nondegenerate chromophore may display substantially different dynamics because the mechanism of coupling to the solvent fluctuations will change. To further investigate the spectral diffusion dynamics in this system, stimulated photon echoes[8] will be used to determine the effects of variable bandwidth excitation on these dynamics. We have recently performed the first condensed phase vibrational stimulated photon echo experiments. The sensitivity of variable bandwidth experiments to the complete population dynamics of a vibrational transition requires a theoretical description of the experimental observable. Detailed theories of spectral diffusion and related observables exist for electronic transitions in very low temperature glasses. New theory for vibrational spectral diffusion in liquids and high temperature glasses is required. Any theories that attempt to explain temperature-dependent vibrational population dynamics will require further insight into the behavior of the density of states for low frequency modes (INMs) of the solvent.

ACKNOWLEDGMENTS

[1] L. J. Muller, D. Vanden Bout, and M. Berg, J. Chem. Phys. **99**, 810 (1993).

[2] D. Zimdars, A. Tokmakoff, S. Chen, S. R. Greenfield, and M. D. Fayer, Phys. Rev. Lett. **70**, 2718 (1993).

[3] A. Tokmakoff, D. Zimdars, B. Sauter, R. S. Francis, A. S. Kwok, and M. D. Fayer, J. Chem. Phys. **101**, 1741 (1994).

[4] A. Tokmakoff, A. S. Kwok, R. S. Urdahl, R. S. Francis, and M. D. Fayer, Chem. Phys. Lett. (to be published).

[5] A. Tokmakoff and M. D. Fayer, J. Chem. Phys. (to be published).

[6] R. F. Loring and S. Mukamel, J. Chem. Phys. **83**, 2116 (1985).

[7] Y. Tanimura and S. Mukamel, J. Chem. Phys. **99**, 9496 (1993).

[8] L. R. Narasimhan, K. A. Littau, D. W. Pack, Y. S. Bai, A. Elschner, and M. D. Fayer, Chem. Rev. **90**, 439 (1990).

[9] D. W. Oxtoby, Adv. Chem. Phys. **47**, 487 (1981).

[10] V. M. Kenkre, A. Tokmakoff, and M. D. Fayer, J. Chem. Phys. (in press).

[11] A. Laubereau and W. Kaiser, Rev. Mod. Phys. **50**, 605 (1978).

[12] N. H. Gottfried and W. Kaiser, Chem. Phys. Lett. **101**, 331 (1983).

[13] H. Graener and A. Laubereau, Chem. Phys. Lett. **133**, 378 (1987).

[14] J. R. Ambroseo and R. M. Hochstrasser, J. Chem. Phys. **89**, 5956 (1988).

[15] S. A. Angel, P. A. Hansen, E. J. Heilweil, and J. C. Stephenson, in *Ultrafast Phenomena VII*, edited by C. B. Harris, E. P. Ippen, G. A. Mourou, and A. H. Zewail (Springer, Berlin, 1990).

[16] H. Graener and G. Seifert, J. Chem. Phys. **98**, 36 (1993).

[17] A. Tokmakoff, B. Sauter, A. S. Kwok, and M. D. Fayer, Chem. Phys. Lett. **221**, 412 (1994).

[18] W. T. Grubbs, T. P. Dougherty, and E. J. Heilweil, Chem. Phys. Lett. **227**, 480 (1994).

[19] S. Califano, V. Schettino, and N. Neto, *Lattice Dynamics of Molecular Crystals* (Springer, Berlin, 1981).

[20] S. Velsko and R. M. Hochstrasser, J. Phys. Chem. **89**, 2240 (1985).

[21] J. Chesnoy and G. M. Gale, Adv. Chem. Phys. **70**, 297 (1988).

[22] J. R. Hill, E. L. Chronister, T.-C. Chang, H. Kim, J. C. Postlewaite, and D. D. Dlott, J. Chem. Phys. **88**, 949 (1988).

[23] J. R. Hill and D. D. Dlott, J. Chem. Phys. **89**, 842 (1988).

[24] A. Tokmakoff, B. Sauter, and M. D. Fayer, J. Chem. Phys. **100**, 9035 (1994).

[25] J. T. Hynes, Annu. Rev. Phys. Chem. **36**, 573 (1985).

[26] R. A. Marcus and N. Sutin, Biochim. Biophys. Acta **811**, 265 (1985).

[27] P. Aechtner and A. Laubereau, Chem. Phys. **419**, 419 (1991).

[28] M. Dubs and H. H. Guenthard, J. Mol. Struct. **60**, 311 (1980).

[29] W. E. Moerner, A. R. Chraplyvy, and A. J. Sievers, Phys. Rev. B **29**, 6694 (1984).

[30] S. P. Love and A. J. Seivers, J. Lumin, **45**, 58 (1990).

[31] H.-G. Cho and H. L. Strauss, J. Chem. Phys. **98**, 2774 (1993).

[32] E. J. Heilweil, M. P. Casassa, R. R. Cavanagh, and J. C. Stephenson, Chem. Phys. Lett. **117**, 185 (1985).

[33] U. Happek, J. R. Engholm, and A. J. Seivers, Chem. Phys. Lett. **221**, 279 (1994).

[34] H. Graener, T. Loesch, and A. Laubereau, J. Chem. Phys. **93**, 5365 (1990).

[35] E. J. Heilweil, R. R. Cavanagh, and J. C. Stephenson, Chem. Phys. Lett. **134**, 181 (1987).

[36] E. J. Heilweil, R. R. Cavanaugh, and J. C. Stephenson, J. Chem. Phys. **89**, 230 (1988).

[37] J. D. Beckerle, M. P. Casassa, R. R. Cavanagh, E. J. Heilweil, and J. C. Stephenson, Chem. Phys. **160**, 487 (1992).

[38] P. Guyot-Sionnest, Phys. Rev. Lett. **66**, 1489 (1991).

[39] A. Tokmakoff, C. D. Marshall, and M. D. Fayer, J. Opt. Soc. Am. B **10**, 1785 (1993).

[40] M. D. Fayer, Annu. Rev. Phys. Chem. **33**, 63 (1982).

[41] G. R. Fleming, *Chemical Applications of Ultrafast Spectroscopy* (Oxford University, New York, 1986).

[42] A. B. Myers and R. M. Hochstrasser, IEEE J. Quantum Electron. **QE-22**, 1482 (1986).

[43] F. W. Deeg and M. D. Fayer, J. Chem. Phys. **91**, 2269 (1989).

[44] C. Alba, L. E. Busse, D. J. List, and C. A. Angell, J. Chem. Phys. **92**, 617 (1990).

[45] S. M. Arrivo, T. P. Dougherty, W. T. Grubbs, and E. J. Heilweil, Chem. Phys. Lett. (submitted).

[46] H. C. Meijers and D. A. Wiersma, Phys. Rev. Lett. **68**, 381 (1992).

[47] D. T. Leeson, O. Berg, and D. A. Wiersma, J. Phys. Chem. **98**, 3913 (1994).

[48] H. Graener, T. Q. Ye, and A. Laubereau, Phys. Rev. B **41**, 2597 (1990).

[49] H. Graener, G. Seifert, and A. Laubereau, Phys. Rev. Lett. **66**, 2092 (1991).

[50] K. Kinosita, Jr., S. Kawato, and A. Ikegami, Biophys. J. **20**, 289 (1977).

[51] G. Lipari and A. Szabo, Biophys. J. **30**, 489 (1980).

[52] G. Lipari and A. Szabo, J. Am. Chem. Soc. **104**, 4546 (1982).

[53] A. Szabo, J. Chem. Phys. **81**, 150 (1984).

[54] M. C. L. Martinez and J. G. de la Torre, Biophys. J. **52**, 303 (1987).

[55] G. Lipari and A. Szabo, J. Chem. Phys. **75**, 2971 (1981).

[56] Viscosity data were compiled from the following sources: A. C. Ling and J. E. Willard, J. Phys. Chem. **72**, 1918 (1968); H. Greenspan and E. Fischer, *ibid*. **69**, 2466 (1965); C. Alba, L. E. Busse, D. J. List, and C. A. Angell, J. Chem. Phys. **92**, 617 (1990).

[57] C. M. Hu and R. Zwanzig, J. Chem. Phys. **60**, 4354 (1974).

[58] L. H. Jones, R. S. McDowell, and M. Goldblatt, Inorg. Chem. **8**, 2349 (1969).

[59] J. Yu and M. Berg, J. Phys. Chem. **97**, 1758 (1993).

[60] K. A. Littau, Y. S. Bai, and M. D. Fayer, Chem. Phys. Lett. **159**, 1 (1989).

[61] W. Breinl, J. Friedrich, and D. Haarer, J. Chem. Phys. **81**, 3915 (1984).

[62] C. Kittel, *Introduction to Solid State Physics* (Wiley, New York, 1976).

[63] P. Moore and T. Keyes, J. Chem. Phys. **100**, 6709 (1993).

[64] P. Moore, A. Tokmakoff, T. Keyes, and M. D. Fayer, J. Chem. Phys. (to be published).

[65] A. Tokmakoff, M. D. Fayer, and D. D. Dlott, J. Phys. Chem. **97**, 1901 (1993).